Detonation Performance Experiments and Modeling for the High Explosive PETN

Eric K. Anderson, Carlos Chiquete, Ritchie I. Chicas
Los Alamos National Laboratory
Los Alamos, NM, USA
Scott I. Jackson
Texas A & M University
College Station, TX USA

1 Introduction

PETN is a commonly used high explosive (HE) for engineering applications. As one of the most sensitive secondary explosives, it is commonly used in detonator, fusing, and booster assemblies. The explosive's sensitivity, high brisance, and small reaction zone allows it to detonate well over a large variation of initial densities. These densities can be adjusted to tune its explosive output to specific needs. For example, PETN at lower densities will undergo DDT more readily [1], making it appealing for use early in explosive trains. PETN is also commonly used as the comparison standard in product equation-of-state (EOS) measurements [2].

Despite its popularity, detailed detonation performance data is relatively sparse for PETN for several reasons. First, the large operational density range of PETN requires a significant amount of tests to characterize experimentally. For example, prior data only addresses three initial densities of 1.263, 1.503 and 1.763 g/cm^3 as derived from cylinder expansion tests (CYLEXs) to characterize the product EOS [2]. Additionally, its short reaction zone [3, 4] requires test assembles to be very small relative to other common explosives (e.g. HMX, Comp B, and TATB) to quantify the effect of confinement and geometry on the explosive performance [5].

There has always been a question as to how small conventional detonation characterization tests (such as rate sticks and cylinder tests) can be made without compromising their ability to deliver useful data due to failure of continuum assumptions. For example, the discrete particles forming the explosive may perturb front curvature measurements at smaller diameters. Another potential problem is that the thin wall associated with scaled down cylinder expansion tests may fail prematurely during expansion due to the presence of an insufficient number of copper grains across the thickness of the wall [6]. In this study, PETN rate sticks and cylinder tests are fielded at the smallest known scales (3-mm HE diameter) at a density of 1.65 g/cc. Analysis yields a Detonation Shock Dynamics (DSD) propagation law and Jones-Wilkens-Lee (JWL) product EOS for programmed burn detonation modeling [7] and to validate reactive flow model calibrations for this explosive [3]. The resulting data verifies that the flow satisfies continuum measurement and analysis methods at these scales, while providing performance calibration data at a previously unreported density. This work also provides the first recorded front shape measurements of PETN.

Correspondence to: eanderson@lanl.gov

2 Experimental

Two unconfined rate sticks and one CYLEX test were fielded, with dimensions as provided in Table 1. All tests were assembled from pressed PETN pellets with a nominal density of 1.65 g/cc. The tests were initiated with RP-2 detonators from Teledyne RISI. Rate stick 8-2179 consisted of 20 PETN pellets glued

Table 1: Test details. Parameters d and L are the explosive assembly diameter and total length. Detonation velocity D_0 from the time of arrival wires or PDV diagnostic is also shown with the $\pm$ standard error.

Identifier	Type	d (mm)	L (mm)	D_0 (mm/μs)
8-2179	rate stick	3.01	50	7.919 ± 0.011
8-2180	rate stick	3.01	50	7.888 ± 0.015
8-2189	CYLEX	3.01	60.2	8.111 ± 0.057

together along their flat faces using Angstrom bond, located in a plastic assembly, and instrumented with ionization wires to measure the time of arrival of the detonation at each wire location as discussed in [5]. During testing, the self-luminescence of the detonation transiting along the long axis of the pellet was imaged with a streak camera in order to provide a high resolution measurement to evaluate the steadiness of the detonation velocity in the rate stick. Rate stick 8-2180 was constructed in a similar manner to 8-2179 but also contained an aluminized window located along the downstream flat face of the pellet assembly to allow for measurement of the detonation shape at the end of the pellet as shown in Fig. 1. Ionization wires were again used as a detonation time-of-arrival diagnostic. Unlike the previous test, however, the streak camera imaged the centerline of the downstream window. During testing, the window was illuminated with light from an argon flash, which was reflected into the streak camera. Arrival of the detonation at the aluminized surface ended this reflection and thus recorded the front shape on the camera film.

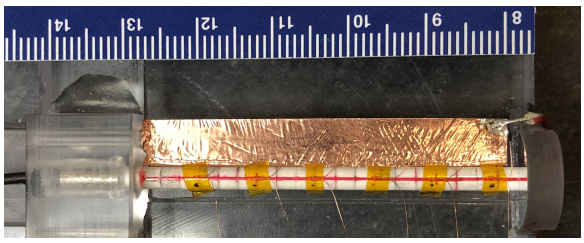

Figure 1: Image of rate stick assembly 8-2180

Cylinder test 8-2189 consisted of an inert confiner tube tightly encasing the assembled rod of PETN. The tube was composed of Oxygen-Free High-Conductivity (OFHC) copper, fabricated through a combination of Electron Discharge Machining (EDM) and conventional machining, and subsequently annealed to a dead-soft temper. The wall thicknesses were scaled down to 1/8.3 of a standard 1-inch cylinder test [6] with an outer diameter of 3.66 mm, an inner diameter of 3.05 mm, and a length of 60.2 mm. The concentricity of the inner and outer diameters were measured and verified to be concentric to within 0.0005 mm. The tube was filled with 24 explosive pellets. Pellet joints and the small gap between the cylinder inner diameter and were filled with Sylgard 184 silicone elastomer to secure the explosive and prevent jetting. The Sylgard layer between the inner copper wall and the HE was inferred to be 20 microns thick.

Eight collimated PDV probes were used to measure the radial motion of the wall during the experiment, were oriented normal to the initial cylinder wall, and were located at seven axial distances from

the detonator–explosive interface of 4.37 (PDV1), 11.91 (PDV2), 19.84 (PDV3), 27.19 (PDV4), 38.50 (PDV5), 43.26 (PDV6 and 7), and 50.8 (PDV8) mm. Two probes were located 180° opposed at the 38.50 mm location. The cylinder test was also equipped with a front-surface window to measure the front shape as was the case with test 8-2180.

3 Experimental Results

All tests yielded full data return. Detonation time-of-arrival data was obtained from the ionization wires in the rate stick tests and from first motion of the PDV probes in the cylinder tests. The steady detonation velocities shown in Table 1 were then obtained by fitting a line to the time-of-arrival and probe location data. The low standard errors associated with these fits for the rate sticks indicate that the detonation wave was steady several diameters away from the detonator-PETN interface. The higher standard error of the cylinder expansion test is to be expected as it is less accurate to use PDV probes as a time-of-arrival diagnostic due to their larger spot size and the inability to characterize their location as precisely as the ionization wires. Analysis of the streak record of test 8-2179 (Fig. 2 (left)) similarly indicated a steady

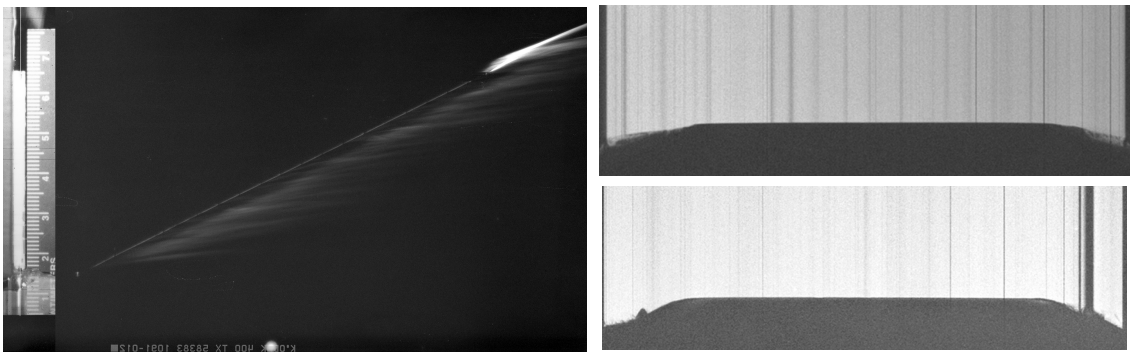

Figure 2: Left: Streak record of rate stick 8-2179. Right: Front breakout traces from tests 8-2180 (top) and 8-2189 (bottom).

detonation velocity that was consistent with the ionization probe measurements. The front shapes from tests 8-2180 and 8-2189 are shown in Fig. 2 (right). These images were analyzed to yield the shape of the detonation front upon breakout from the downstream surface of the cylinder. The results are shown in Fig. 3 (left). The fronts appeared smooth in all tests, indicating continuum behavior.

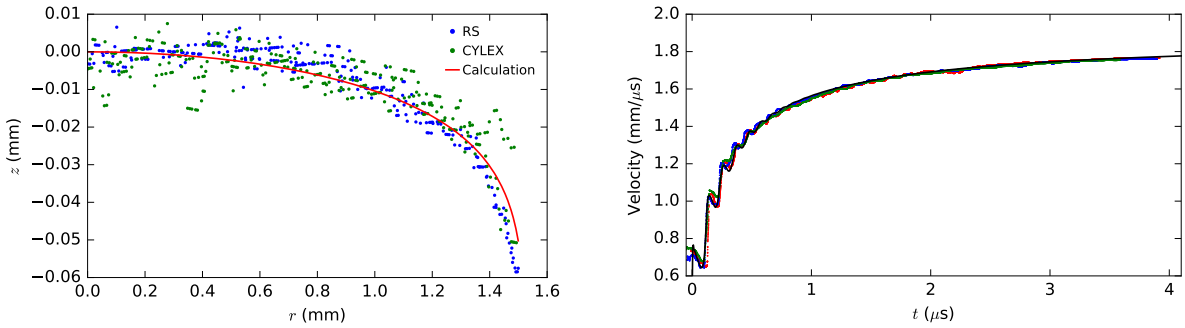

Figure 3: Left: Front shapes (after a symmetrization process) from tests 8-2180 (green) and 8-2189 (blue) with DSD model prediction (red). Right: PDV profiles from cylinder expansion test 8-2189. Colored lines indicate individual PDV2–PDV4. The black line is the fitted calculation from the model.

The PDV wall velocity histories are shown in Fig. 3 (right). The cylinder exhibited very good expansion despite its exceptionally thin wall thickness of 0.31 mm. Records PDV2, PDV3, and PDV4 exhibited the longest motion records and were used in the modeling analysis.

4 Modeling analysis

Our model analysis uses a modern programmed burn model for calibration of PETN at 1.65 g/cm^3 [8]). Our chosen methodologies to represent the timing and energy release are DSD and VAJWL, respectively.

4.1 Timing model

Detonation Shock Dynamics (DSD) relates the local detonation velocity D_n to local shock front curvature κ and is calibrated from the rate stick phase velocities and front shapes [9]. The recorded front data in this work are the first reported such measurements for this explosive at any density and offer the first opportunity to determine this model parameter for this commonly-used explosive. The DSD calibration methodology followed is detailed and validated extensively in Chiquete et al. [8] for PBX 9501, an ideal HMX-based explosive.

The DSD propagation law is $D_n(\kappa) = D_{CJ}(1 - B\kappa)$ and analysis determined the optimal $D_n - \kappa$ parameters are $D_{CJ} = 7.905$ mm/μs, $B = 0.0069844$ mm with an unconfined or sonic edge angle of 30 degrees. The B parameter in this relationship is correlated to the reaction zone length via an asymptotic analysis [7] and is nearly 10 times smaller for PETN than for PBX 9501 [8], indicating that the PETN reaction zone length is on the order of microns. Figure 3 (left) compares the unconfined DSD front shape calculation to the recorded front shapes for the rate stick and CYLEX tests. The experimental front shapes were symmetrized following the procedure in [8]. The similarity between the unconfined calculation and the CYLEX data indicates that the PETN reaction zone did not experience significant confinement from the copper wall, likely due to the 20-micron-thick Sylgard layer being several times the PETN reaction zone length. Due to this observation, DSD timing calculations of the CYLEX geometry assumed unconfined detonation-wall interactions and used the sonic edge angle as the boundary condition. Figure 3 (left) also shows stochastic variations on the order of $\pm$ 10 microns, which is a relatively large proportion of the total front deflection (about 60 microns) for these measurements. These variations may be correlated to the representative crystal grain size for a given explosive [8].

4.2 Energy release model

Programmed burn models also require subscale models to predict both the detonation front shape evolution and to characterize the work done by the detonation products. This study uses the VAJWL energy release method [8], which is a modification of the Jones-Wilkins-Lee (JWL) equation-of-state [10] that is specifically augmented with energy deposition offsets that depend on the local, spatially-dependent normal velocity (D_n) and time of arrival (t_b) derived from DSD. The energy release model modifies the pressure (p) dependence on the local specific energy (e) and volume (v),

$$p(v,e) = (A + a(D_n))\left(1 - \frac{\omega v_0}{(R_1 + r_1(D_n))v}\right) \times \exp\left(-\frac{(R_1 + r_1(D_n))v}{v_0}\right) + B\left(1 - \frac{\omega v_0}{R_2 v}\right) \times \exp\left(-\frac{R_2 v}{v_0}\right) + \frac{\omega}{v}(e - e' - \lambda(t_b)E_{det}),$$

where A, B, R_1, R_2, E_{det} and ω are the base EOS model parameters, a and R_1 are curvature-dependent perturbations, e' is a constant of integration such that $p(v_0, 0) = 0$ (standard convention in condensed-phase detonation where the ambient pressure is negligible relative to the post-shock values).

Our iterative hydrocode-based process solves for the energy release and products EOS parameters of this model [11, 12, 13] and is constrained by the PDV wall motion records. The error metric is based on the RMS error of the comparison between data and calculation. The utilized resolution is 31.25 microns and A, B, R_1, R_2 were optimized while ω was kept fixed and E_{det} was used to enforce $D_{CJ} = 7.905$ mm/μs for consistency with the $D_n - \kappa$ law. The result of numerical minimization of this function appears in Fig. 3 (right) and the parameters appear in Table 2. The product EOS parameters in Table 2 are an excellent fit to the experimental data.

Table 2: The calibrated EOS parameters. The CJ state velocity, pressure and specific volume are 7.905 mm/μs, 28.36 GPa, and 0.4394 cm^3/g, respectively.

A (GPa)	B (GPa)	R_1	R_2	C (GPa)	ω	E_{det} (kJ/g)	ρ_0 (g/cm^3)
521.078	15.836	4.492	1.444	1.793	0.3043	6.616	1.650

The present results can be compared to prior PETN measurements at other pressing densities. Figure 4 includes the product isentropes in pressure (left) and energy (right, as offset by the Rayleigh energy $1/2 p_{CJ}(v_0 - v_{CJ})$) for the present density of 1.65 g/cc along with those from Souers and Kury [2] for 1.263, 1.503 and 1.763 g/cm^3. The isentropes are seen to scale well with initial density. The P–v plot also shows that the CJ pressure and density increase with ρ_0.

There are several differences between the present study and prior work. The EOS models from [2] were (1) derived from cylinder expansion experiments tracking the radial expansion at a given axial location via streak camera, using (2) much larger HE pellet diameters of 25.4 mm (nearly 8.3 times as thick as in the present ones), and (3) using copper wall thicknesses of 1.36 and 2.59 mms (as compared to 0.3 mm in the present tests). Despite these substantial scale and diagnostic differences, the combined results scale consistently and indicate that the explosive density is the dominant scaling parameter affecting detonation performance for this ideal explosive formulation.

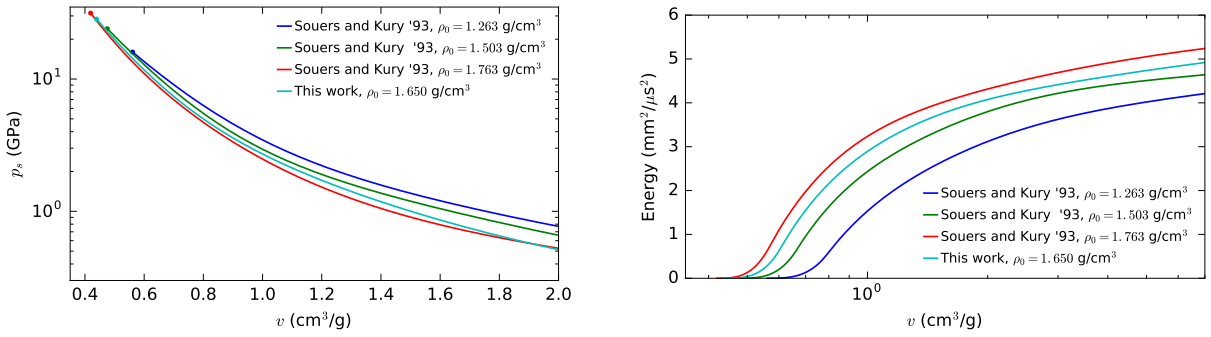

Figure 4: Top left: Product EOS isentrope variation with density. Circles represent CJ values. Bottom right: The corresponding energy delivery with density.

References

[1] P. Schulze, I. Lopez-Pulliam, E. Heatwole, T. Feagin, and G. Parker. The deflagration-to-detonation transition (DDT) in high density pentaerythritol tetranitrate (PETN). In *AIP Conf. Proc.*, volume 2272, page 050027. AIP Publishing LLC, 2020.

[2] P. C. Souers and J. W. Kury. Comparison of cylinder data and code calculations for homogeneous explosives. *Prop. Expl. Pyro.*, 18(4):175–183, 1993.

[3] T. D. Aslam, C. A. Bolme, K. J. Ramos, M. J. Cawkwell, C. Ticknor, M. A. Price, J. A. Leiding, N. J. Sanchez, and S. A. Andrews. Shock to detonation transition of pentaerythritol tetranitrate (PETN) initially pressed to 1.65 g/cm^3. *J. Appl. Phys.*, 130(2):025901, 2021.

[4] A. S. Tappan, R. Knepper, R. R. Wixom, J. C. Miller, M. P. Marquez, and J. P. Ball. Critical thickness measurements in vapor-deposited pentaerythritol tetranitrate (PETN) films. In *Proc. 14th Intl. Symp. on Detonation*, pages 11–16, 2010.

[5] S. I. Jackson and M. Short. Scaling of detonation velocity in cylinder and slab geometries for ideal, insensitive and non-ideal explosives. *J. Fluid Mech.*, 773:224–266, 2015.

[6] S. I. Jackson. Scaled cylinder test experiments with insensitive PBX 9502 explosive. In *Proc. 15th Intl. Det. Symp.* Office of Naval Research, 2015.

[7] J. B. Bdzil and D. S. Stewart. The dynamics of detonation in explosive systems. *Annu. Rev. Fluid Mech.*, 39:263–292, 2007.

[8] C. Chiquete, M. Short, E. K. Anderson, and S. I. Jackson. Detonation shock dynamics modeling and calibration of the HMX-based conventional high explosive PBX 9501 with application to the two-dimensional circular arc geometry. *Combust. Flame*, 222:213–232, 2020.

[9] J. B. Bdzil, W. Fickett, and D. S. Stewart. Detonation shock dynamics: a new approach to modeling multi-dimensional detonation waves. In *Proc. 9th Intl. Symp. on Detonation*, pages 730–42, 1989.

[10] E. Lee, M. Finger, and W. Collins. JWL equation of state coefficients for high explosives. Technical Report UCID-16189, Lawrence Livermore National Laboratory, 1973.

[11] C. Chiquete and S. I. Jackson. Detonation performance of the CL-20-based explosive LX-19. *Proc. Combust. Instit.*, 38(3):3661–3669, 2020. doi: https://doi.org/10.1016/j.proci.2020.07.089.

[12] C. Chiquete, S. I. Jackson, E. K. Anderson, and M. Short. Detonation performance experiments and modeling for the DAAF-based high explosive PBX 9701. *Combust. Flame*, 223:382–397, 2020. doi: https://doi.org/10.1016/j.combustflame.2020.10.009.

[13] E. K. Anderson, C. Chiquete, S. I. Jackson, R. I. Chicas, and M. Short. The comparative effect of HMX content on the detonation performance characterization of PBX 9012 and PBX 9501 high explosives. *Combust. Flame*, 230:111415, 2021.